Temporal Vascular Endothelial Growth Factor Sub-type gene Switching in SARS-CoV Pathogenesis. Interpretation through in vivo Murine C57BL Models

Asrar Rashid[1,2], Zainab A. Malik[5,6], Varun Sharma[7], Anuka Sharma[7], Love Gupta[7], Hoda Alkhazaimi[8], Guftar Shaikh[9], Ahmed Al-Dubai[1], Amir Hussain[1]

1. School of Computing, Edinburgh Napier University. Edinburgh, UK.
2. NMC Royal Hospital. Abu Dhabi, UAE.
3. Weill Cornell Medicine-Qatar. Doha, Qatar.
4. Institute of Cardiovascular Science, University of Manchester. Manchester, UK.
5. College of Medicine, Mohammed Bin Rashid University of Medicine and Health Sciences. Dubai, U.A.E.
6. Mediclinic City Hospital. Dubai, UAE.
7. NMC Genetics
8. New York University Abu Dhabi, UAE
9. Endocrinology, Royal Hospital for Children. Glasgow, UK.

*Corresponding author Dr. Asrar Rashid asrar.rashid@napier.ac.uk

Temporal Vascular Endothelial Growth Factor Sub-type gene Switching in SARS-CoV Pathogenesis, Interpretation through In-vivo Murine C57BL Models

Introduction

Increased Vascular Endothelial Growth Factor A (VEGF-A) levels are associated with Severe Acute Respiratory (SARS) infection. The aim was to investigate in vivo VEGF-A and VEGF-B (VEGF-A/B) gene expression (GE) in severe pulmonary disease pathogenesis.

Method

Twelve temporal Mus musculus Wildtype (WT) C57BL/6 SARS-CoV MA15 lung studies were selected from the NCBI GEO database for GE profiling.

Results

In murine dataset (GSE68820) Day 2 was compared to Day 7 demonstrating a downregulation trend in VEGF-A GE, with an opposite effect on VEGF-B GE (p=4.147e-03, p=7.580e-07, respectively). A ‘v-shaped VEGF-B gene expression trajectory was noteworthy across certain datasets and after dORF6 stimulation. In addition, MA15 dose stimulation studies showed that a higher antigenic load caused more profound effects on VEGF-A resulting in a steeper fall in GE compared to other antigens.

Conclusions

Distinct temporal trajectory patterns of VEGF-A and VEGF-B gene expression were associated with SARS-CoV MA15 stimulation. Unraveling the importance of VEG-A/B dynamics offers exciting prospects for improved bio-marking and therapeutic precision.

Keywords

SARS, SARS-CoV2, Vasoactive Endothelial Growth Factor, VEGF-A, VEGF-B

Introduction

Coronaviruses cause Severe Acute Respiratory Syndrome (SARS), with SARS-CoV-2 responsible for the recent Novel Coronavirus Disease 2019 (Covid-19) pandemic. Severe pulmonary disease is an important consequence of SARS-CoV-2 infection, causing Acute Respiratory Distress (ARDS) in adult patients infected with Covid-19. Mortality from severe pulmonary infection is highest among at-risk groups with chronic underlying conditions, including those with obesity and hypertension [1,2]. Several mechanisms predisposing to severe Covid-19 infection have been explored, including the role of SARS-CoV2 spike protein [3] and the Vascular Endothelial Growth Factor (VEGF) [4]. Chi et al. (2020) demonstrated increased levels of VEGF in 70 patients infected with SARS-CoV2 infection compared to controls [5]. In the same study, a decreased temporal trend was noted in VEGF-A protein levels from acute symptomatic to convalescence. This suggests that VEGF levels are increased in the setting of clinical SARS-CoV-2 infection, decreasing with clinical improvement.

The VEGF protein consists of several sub-classes, including VEGF-A, VEGF-B, VEGF-C, VEGF-D, VEGF-E, and placental growth factor [6]. VEGF-A was the first VEGF sub-class to be characterized, providing the basis for anti-angiogenesis as a therapeutic strategy, including the clinical development of bevacizumab, a humanized monoclonal antibody acting against VEGF-A[7]. VEGF proteins binding to VEGF receptors may have physiological implications. For example, VEGF-A binding to VEGF Receptor 1 (VEGFR-1) has an insignificant effect on receptor activation, with VEGFR-1 acting as a decoy and VEGF-B binding to VEGFR-1 promoting cell survival [8]. VEGF-A also binds to VEGF Receptor 2 (VEGFR-2), albeit with a lower affinity, resulting in endothelial cell migration and proliferation. VEGF-A binding to VEGFR2 is considered an essential transducer for

angiogenesis. A high number of VEGFR2 receptors are expressed in pulmonary tissue, implying the importance of VEGF-A in health and disease [9].

The MYSTIC study demonstrated increased levels of VEGF-A and VEGF-D subtypes in Covid-19 ventilated versus non-ventilated patients [10]. Increased VEGF-A binding to VEGFR receptors also enhances vascular permeability, contributing to disease pathogenesis. The basis for the severe disease after SARS-CoV infection and its relationship to VEGF-A is not simply related to pulmonary bed fluid status. For example, sub-optimal clinical hydration practiced during the early phase of the pandemic was detrimental and linked to increased VEGF expression[11], leading to the stimulation of angiogenesis, increase in vascular permeability and nitric oxide-mediated vasodilatation[11]. VEGF-B levels are found to be the highest in high metabolic activity tissues, including brown adipose, heart, and skeletal muscle. VEGF-A and VEGF-B both bind to VEGR-1 with their interaction of potential homeostatic importance. For example, in metabolic homeostasis, VEFG-B binding to VEGFR-1 is associated with the activation of the VEGF-A VEGFR-2 pathway[12]. The idea that VEGF-B might displace VEGF-A from the VEGF-R1, causing a shift of VEGF-A to VEGF-R2, is one possibility that has also been suggested in studies of nonhereditary, non-metastatic pheochromocytoma[13]. The association of VEGF-A levels with Covid-19 pulmonary disease and angiogenesis has been explored. In a post-mortem study of patients with Covid-19, pulmonary tissue showed luminal cylindrical microstructure formation in capillaries and intussusceptive angiogenesis (IA) [14]. VEGF-A signaling plays an important role in COVID-19-related IA, resulting in endothelial mitogenesis, differentiation, and migration [15]. This suggests that VEGF-A could be an important component in Covid-19 associated angiogenesis.

VEGF-A has pro-inflammatory effects worse in severe SARS-CoV-2

in pulmonary disease. VEGF-A inflammation occurs at three junctures in the disease pathway [16]. Initially, the VEFG-A stimulating activation of IL-6 mediation results in STAT-3 release, which creates an autofeedback loop amplifying further VEGF-A production. This is followed by an Akt pathway which supports feedback loop secretion via the IL-6/STAT-3 pathway. Finally, VEGF-A activates NF-κB in its role as a pro-inflammatory molecule. VEGF-B is co-expressed with VEGF-A across tissues but showing a particular abundance in heart and skeletal muscle [17]. In contrast to VEGF-A, the role of VEGF-B in SARS-CoV-2 disease pathogenesis has not been characterized in SARS-CoV-2 infection. However, SARS-CoV-2 has been associated with a Kawasaki Disease (KD) phenotype in children, occurring a few weeks after primary infection. Further, in non-SARS-CoV-2 KD, international studies have shown VEGF-A and VEGF-B gene expression to have a consistent inverse relationship [18]. This led to the introduction of the idea of temporal VEFG-A and VEGF-B switching in KD, associated with changes in TNF and NFKB1 gene expression.

In this paper, we wish to explore VEGF-A and VEGF-B gene expression in further detail using a suitable SARS-CoV in vivo model. There are several publicly available transcriptomic datasets studying the effects of SARS CoV MA15 nasal instillation on C57BL Wild Type (WT) mice. Here, a SARS-CoV Murine Model using the Murine A15 (MA15) virus, was developed by researchers through the serial passage in the respiratory tract of young BALB/c mice by the SARS-CoV virus (Urbani strain). MA15 by intranasal inoculation is lethal in mice [19]. The SARS MA15 antigen is especially immunogenic when instilled nasally. MA15 instillation results in rapid viremia and high-titer viral replication in the lungs, and extra-pulmonary dissemination in mice. This is accompanied by lymphopenia and

neutrophilia, associated with pulmonary pathology. The aim of this paper was to document patterns in VEGF-A and VEGF-B gene expression in the Murine MA15 Pulmonary model in WT mice to be able to offer insights into human SARS-CoV pulmonary infection.

Material and Methods

Dataset Selection

Temporal Gene Expression (GE) datasets were chosen from the NCBI GEO database and included temporal studies of murine pulmonary infection with MA15 coronavirus. Models used intranasal instillation of Plaque Forming Units (PFU) of SARS MA15 phosphate-buffered saline (PBS) or mock-infected (control samples) with PBS alone. Analysis of MA15 SARS-CoV infection was limited to Murine Wildtype C57BL/6 (WT) lung studies. Datasets with samples from more than one-time point were included. A search strategy seeking SARS-related data was divided into two. One strategy focused on recovering publicly available microarray experiments, and the other on RNAseq transcriptome SARS-associated datasets. The First Search Strategy included "SARS" as the input term was parsed through the EMBL-EBI(https://www.ebi.ac.uk/) database. Additionally, for the NCBI GEO datasets (https://www.ncbi.nlm.nih.gov/gds), Homo sapiens were selected in the species selection. Out of 248 and 34 entries in the datasets,15 were selected. Hence 12 microarray datasets were selected using the search strategy (Figure 1). A second strategy to ensure the inclusion of RNA-seq studies did not yield eligible datasets.

In Silico Analysis

Statistical and Gene Ontology analyses

Qlucore Omics Explorer (QOE) version 3.7 software (Qlucore AB, Lund, Sweden) was used for the Differential Expression of the Genes (DEGs) analysis. Principal Component Analysis (PCA) plots were generated using QOE. Two-group and multi-group (ANOVA) comparisons, as well as unsupervised hierarchical clustering, were

undertaken in QOE. Gene Symbols were generated for the gene probes. To correct for the multiple results for some probes with the same Gene Symbol, averaging of the expression data was undertaken on all microarray datasets before box-plot analysis and GSEA. Genes were scaled to variance equal to one and centered to mean equal to zero. The False discovery rate (FDR), 'q', was used in the analysis. A value of below 0.25 was considered statistically significant for the FDR. Euclidean distance and average linkage clustering were the basis for Hierarchical clustering in QOE. All microarray data was log2 quantile normalized. VEGF-A protein data bank structure receptor 1WDF and SARS-CoV spike protein-ligand 1BJ1 were selected for protein docking using Barcelona supercomputing server tool pyDOC (PMID: 23661696). Over one hundred variants from this receptor and ligand were selected for further analyses. Top hits from prediction models were plotted using Pymol[20]. The student t-test was used to compare gene expression between groups of samples, with a student p-value of <0.05 being defined as being statistically significant.

Transcript Time Course Analysis

Transcript Time Course Analysis (TTCA) R software was used [21] for temporal data analysis. Curation of VEGFA, VEGFB, TNF, and NFKB1 gene expression was undertaken using the Hugo database. Over-representation analyses (via hypergeometric-distribution-based testing) were performed using the TTCA-generated results. This represented significant genes according to 'Consensus,' 'Early Response,' 'Middle Response,' 'Late Response,' 'Complete Response,' 'Dynamic,' and 'MaxDist.'

Results

A. MURINE SARS Temporal Gene Expression Analysis

The twelve Murine datasets selected from the search were analyzed for changes in gene expression. Four datasets (GSE51387, GSE51386, GSE50878, GSE40827) did not show significant differences in VEGF-A and VEGF-B gene expression across time points with Mock or MA15 stimulation. Due to only one time-point for mock versus MA15 stimulation at 5 Days Post Instillation (DPI), temporal t-test analysis was not possible for one dataset (GSE36016) and was thus excluded from further analysis. Subsequently, datasets showing significant differences in temporal gene expression included GSE68820 (Figure 2), GSE33266 (Figure 3), GSE50000 (Figure 5), and four further datasets (Figure 4).

Box-plot analysis showed temporal changes in VEGF-A and VEGF-B gene expression for the dataset GSE68820 (Figure 2A). Temporal trends 1 to 7 DPI of MA15 suggested an inverse association between VEGF-A and VEGF-B GE. TNF and NFKB1 gene expression also tended downwards over the study period, suggesting that as inflammatory subsides VEGF-B levels rise. Trends in TTCA also suggested similar gene expression patterns compared to controls, though initial NFKB1 gene expression compared to controls was separated, converging by day 4 (Figure 2B). Then, a t-test comparison of 2 to 7 DPI elicited 922 genes. Enrichment of these genes was then undertaken according to BioCarta2016 (Figure 2D) and Covid-19-related Gene Sets 2021 (Figure 2E). These showed IL-6 signaling pathway enrichment as well as several Covid-19 protein pathways. In the latter, SARS coronavirus P2 envelope protein enrichment was also noted. Suggesting an overlap in pathogenesis in the SARS-CoV MA15 virus and SARS-CoV-2.

B. MURINE SARS Gene Expression Analysis, dose study (GSE33266)

Dataset GSE33266 allowed illustration of MA15 dose-dependent antigenic stimulation in the Murine MA15 WT Pulmonary model. Changes in VEGF-A and VEGF-B (Day 1 to Day 7) gene expression were noted (Figure 3). However, at the 10^4 and 10^5 dosing, a v-shape in VEGF-B GE was noted on Day 1, Day 2, and Day 4 vertices. Representing a fall and then an increase in VEGF-B GE. TTCA patterns suggest a trend towards VEGF-A GE divergence between Mock and cases at all doses of MA15. A divergent trend is also noted for VEGF-B GE though the 10^4 MA15 dosing suggests a trend toward convergence.

C. Comparing the 10^4 and 10^5 doses in MURINE SARS Gene Expression Analysis

The 10^4 and 10^5 MA15 doses were individualy tested against Mock (Figure 5). Here mock shows no change in VEGF-A or VEGF-B GE after MA15 stimulation. At both the 10^4 and 10^5 doses, VEGF-A was seen to trend downwards across the study period. However, the 10^5 dose shows a stepwise fall in VEGF-A GE at each DPI interval time point, implying a greater downward effect as the 10^4 MA15 dose did not elicit such as stepped fall in GE.

D. PROTEIN-PROTEIN DOCKING

The pyDOC platform predicted the best docking models between VEGF receptors and SARS-CoV spike protein. The best models were calculated and ranked based on electrostatics and desolvation energy (Table 2). All predicted models were extracted and plotted to estimate the stability of interaction. Interestingly, the top predicted models demonstrated stable interaction between receptors of VEGF and spike protein of SARS-CoV (Figures 6A-6J).

DISCUSSION

This paper aimed to advance the understanding of VEGF-A and VEGF-B changes in gene expression (GE) associated with SARS pathogenesis. Thus a Murine WT SARS-CoV MA15 pulmonary disease model was used to analyze VEGF-A and VEGF-B GE patterns. A systematic search of the NCBI Geo database generated twelve gene expression datasets for analysis. In one dataset, a significant fall in VEGF-A GE associated with a rise in VEGF-B GE was noted (dataset GSE68820); this was also associated with a fall in TNF GE (Figure 2). Given the fact that VEGF-A and VEGF-B share the receptor VEGFR-1, we suggest that these temporal findings imply an inverse relationship between VEGF-A and VEGF-B genes. From the same dataset, a temporal comparison of gene expression revealed enrichment for pathways related to Human Covid19. Showing MA15 studies in the Murine SARS-CoV model to cause pathogenesis representative of Human Covid-19 infection. In temporal MA15 dose analysis (GSE33266), a fall in both VEGF-A and VEGF-B gene expression was noted. Analysis of another temporal dataset (GSE50000) showed that the higher (10^5 versus 10^4) MA15 dose caused a more significant fall in VEGF-A GE. In this dataset, there were no changes in VEGF-B GE. Further, analysis of other murine datasets (GSE40840, GSE40824, GSE49262, GSE49263) showed a tendency towards a temporal fall in VEGF-A GE. Clinical studies show an elevation of VEGF-A protein in severe pulmonary disease associated with SARS-CoV-19[5]. Therefore acute infection is likely to be followed by a temporal reduction in VEGF-A protein levels after coronavirus infection. Also, when comparing differing antigens, MA15 was found to have a strong immunogenic effect, resulting in a steep fall in GE. A v-shape change in VEGF-B GE was noted with dORF6 antigen stimulation, signifying a fall followed by an increase in VEGF-B GE

over the 4-day study period. This v-shape was also noted in the MA15 dose-association study (GSE33266) at 10^4 and 10^5 doses. Thus a temporal fall in VEGF-A GE remains a consistent phenomenon after MA15 dosing.

Studying the status of VEGF proteins in severe pulmonary disease can provide an idea of the differential host effects of VEGF-A and VEGF-B. Based on the clinical literature, elevated VEGF-A protein levels are associated with severe SARS. However, little is known about the function of VEGF-B in pulmonary disease. Unlike VEGF-A, studies show that VEGF-B does not induce angiogenesis in many organs[22]. The receptor interaction of VEGFA/B proteins may be helpful in defining pathophysiological effects. However, VEGF-A and VEGF-B have a complex interaction based on differential receptor affinity and feedback system [23]. VEGFR-1 binds to both VEGF-A and VEGF-B, but VEGR-2 only binds to VEGFR-A. The end molecular effect is based on protein receptor binding to either VEGFR1 or VEGFR2, the latter known as the angiogenic receptor. Also, VEGFR1 or VEGFR2 have a differential affinity for VEGF-A. VEGFR1 demonstrates a 10x higher affinity for VEGF-A compared to VEGFR2. VEGF-B shows preferential binding to VEGFR1 and can displace VEGF-A, resulting in increased VEGFR2 binding of VEGF-A. The role of VEGF-B may be more important for cellular survival, given its anti-apoptotic effects. VEGF-B has been implicated in cardio-protection, causing cardiac hypertrophy, minimizing cellular death, and increasing artery size and capillary diameter[23]. As such, a cardiac role for VEGF-B is concordant with VEGF-B receptor preponderance in the heart[17]. Based on findings from this paper, we present a VEGF-A and VEGF-B disease model, incorporating dynamic changes in gene expression (Figure 7). Assuming temporal changes in VEGF-A and VEGF-B GE reflect VEGF-A/B protein mediation on pulmonary host tissue, two states are

suggested. Ranging from acute inflammation with VEGF-A preponderance and angiogenesis; to that associated with elevated VEGF-B and cellular protection.

To appreciate temporal effects in gene expression, two methods were adopted to understand GE time-related dynamics. One method involves the t-test comparing time points to generate box plots, and the second method involves the application of TTCA software. This is the first study (we believe) using TTCA in viral sepsis, allowing a comparison with temporal box plots. TTCA was designed to cater to dynamic changes in GE. Thus this tool is suited to acute temporal sepsis microarray studies, given the dynamic changes that occur. For statistical box plot analysis, the t-test provides an objective measure of change in gene expression. At the same time, TTCA gives a visual interpretation of changes in GE. Dose-dependent (GSE33266) TTCA patterns showed that MA15 stimulation changed NFKB1 and TNF GE, consistent with increased inflammation when then subsided over time. Temporal changes may have clinical implications. For example, sample timing should be cognizant of the timing of inflammation.

The emphasis of our study was to understand VEGF-A and VEGF-B changes in GE. If the behavior of VEGF-A and VEGF-B genes can be correlated to their respective proteins, gene expression data may have many applications, from understanding disease pathogenies to providing an opportunity to follow therapeutic effects. Thus, supporting the idea of using changing GE from a biomarker perspective. However, some murine studies did not elicit changes in VEGF-A or VEGF-B GE after either Mock or MA15 stimulation. The consistency of the absence of changes in cases versus controls suggests differences that could be related to experimental nuances, such as antigen stimulation and sampling techniques. We also showed that the SARS-CoV-2 Spike protein has the potential to bind directly to

VEGF-associated receptors (Figure 6). The SARS-CoV-2 spike protein may lead to pathophysiological consequences through other mechanisms. For example, SARS-CoV-2 spike protein can co-op the VEGF-A/neuropilin-1 receptor inducing analgesia[24]. Based on our modeling, if SARS-CoV MA15 protein receptor binding to VEGFR1/VEGFR2 is akin to that of SARS-CoV-2, this could interfere with existing feedback loops regulating VEGFA/B. The idea that the MA15 viral protein itself may elicit pro-inflammatory effects through VEGF-R2 binding requires validation in future works.

Regarding the issue of translation of murine studies to the clinical arena, two points are noted in our paper. Firstly, the VEGF-B amino acid sequence has 88% homology between mice and humans[17]. Secondly, the analysis showed that, in the murine MA15 nasal instillation model, pathways suggestive of human SARS-CoV-2 disease were also enriched. These points support the use of the murine model in ascertaining a human pathophysiological perspective. VEGF-A and VEGF-B are homologs, share a receptor (VEGFR-1), and have shown patterns that might suggest a close relationship. This study has shown the value of microarray time series analysis in developing a perspective on an evolving disease process. An advantage of in vivo research is the ability to both control the commencement of the experiment and incorporate controls. However, to gain similar value in clinical gene expression research, the idea of multiple sampling points should be a consideration for future clinical studies. Currently, there is a paucity of clinical temporal GE data with point-by-point microarray being used mainly for prediction and classification, not disease evolution. On the idea of novel therapeutics, this study suggests the potential to manipulate VEGF-A and VEGF-B after coronavirus infection. The dual relationship between VEGF-A-associated pro-inflammation and enhanced survival

by VEGF-B could be explored from a clinical perspective. VEGF-A binds to VEGFR-2, whereas VEGF-B does not. The protein-receptor binding configuration could be explored for clinical benefit. For example, Behelgardi et al. (2018) designed a VEGFR1 and VEGFR2 binding protein, termed VGB4, with anti-angiogenic and anti-tumor properties applied to a Murine model [25]. Sadremomtaz et al. (2020) also developed a VEGF receptor binding peptide, VGB3, with high-affinity binding and neutralization of a second extracellular domain of VEGFR1D2 [26]. In this work, VGB3 was designed to disrupt the VEGFB–VEGFA/VEGFR1D2-associated angiogenesis and resulted in both anti-angiogenic and anti-tumor effects. Modeling of high-affinity binding peptides to VEGFR2 was attempted by Ghasemali et al. (2022) as a possible mechanism to inhibit VEGF/VEGFR2 angiogenesis[27]. In the future, therapies could be designed, and efficacy tested according to changes in VEGF-A and VEGF-B GE and associated trajectories. For example, gene therapy was attempted in the porcine heart using VEGF-B, hoping to facilitate change for myocardial benefit [28]. However, the researchers noted that inflammatory responses attenuated the therapeutic effect of their gene transfer vector. A significant reduction in successful transduction and long-term gene expression occurred, even despite immunosuppression and optimization of gene transfer methods. Understanding VEGF-A and VEG-B gene expression changes could have provided vital insights. Thus, given the findings of our paper, VEGF-A/B cellular interactions should be taken into account, noting temporal differences, especially when considering an impact on angiogenesis.

Figure 1. Search Strategy for Gene Expression analysis in Murine MA15 Pulmonary Infection Studies

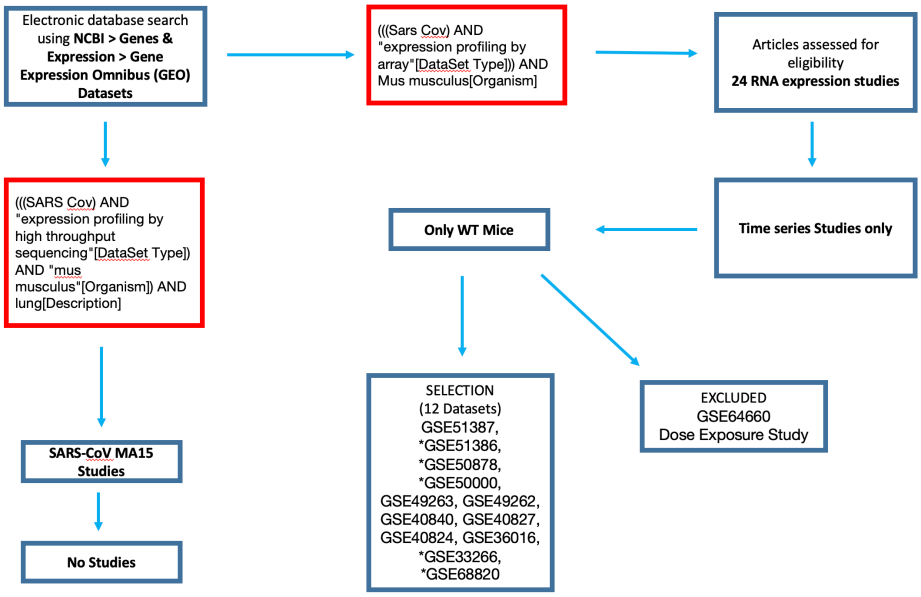

Figure 1. The search strategy undertaken on the 26th August 2022, used the NCBI GEO database as shown. The goal was to identify studies which used, a one event MA15 antigenic stimulation of the Murine respiratory tract. Thus search criteria contained the following terms: (((Sars Cov) AND "expression profiling by array"[DataSet Type])) AND Mus musculus[Organism]. 24 items were found in which 8 datasets researched non-temporal post Murine MA15 SARS CoV infection, thus were excluded from further analysis. Further, 3 of the 16 datasets were not related to WT mice and were eliminated. Also excluded was dataset GSE64660, aiming to understand the effects of prolonged host exposure to MA15.In order to ensure the inclusion of RNA-seq datasets the following search criteria was applied to the NCBI dataset search : (SARS CoV) AND "expression profiling by high throughput sequencing"[DataSet Type]) AND "mus musculus"[Organism]) AND lung[Description]. All datasets generated were deemed ineligible as they did not include WT data, were not time series, and were not related to a pulmonary SARS disease model.

Figure 2. A study of Pulmonary Gene Expression in Murine (WT) Model with CoV virus nasal instillation of MA15 versus Mock.

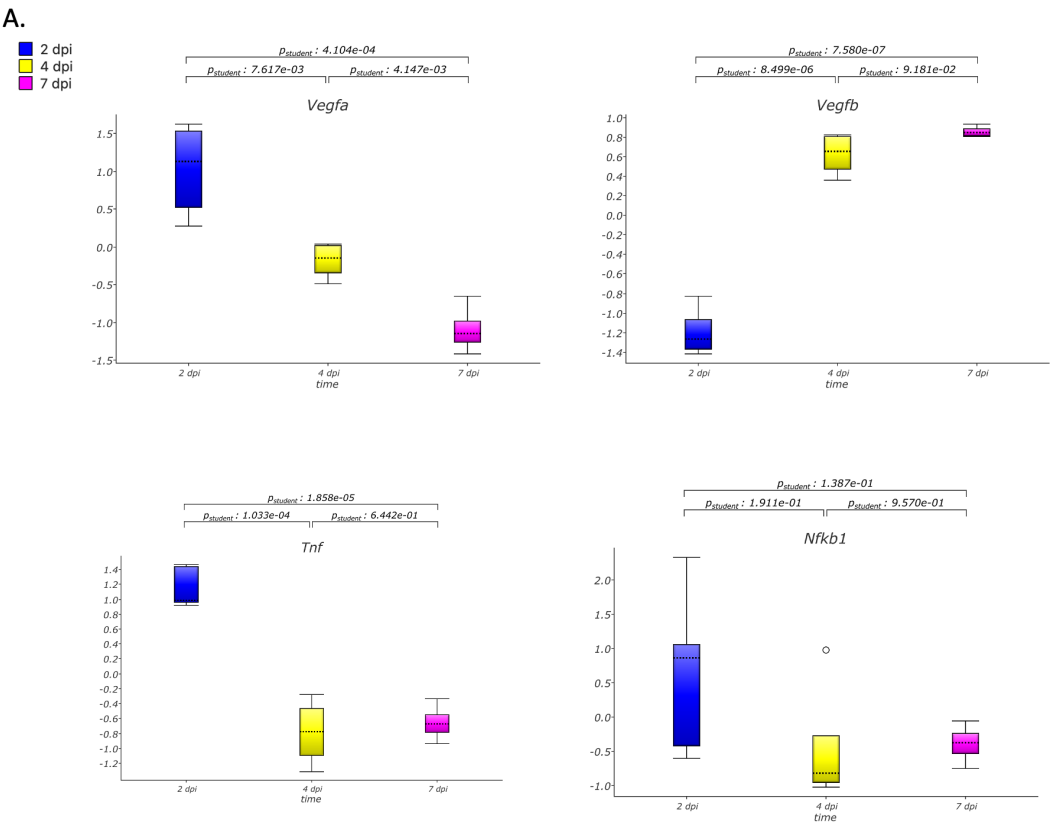

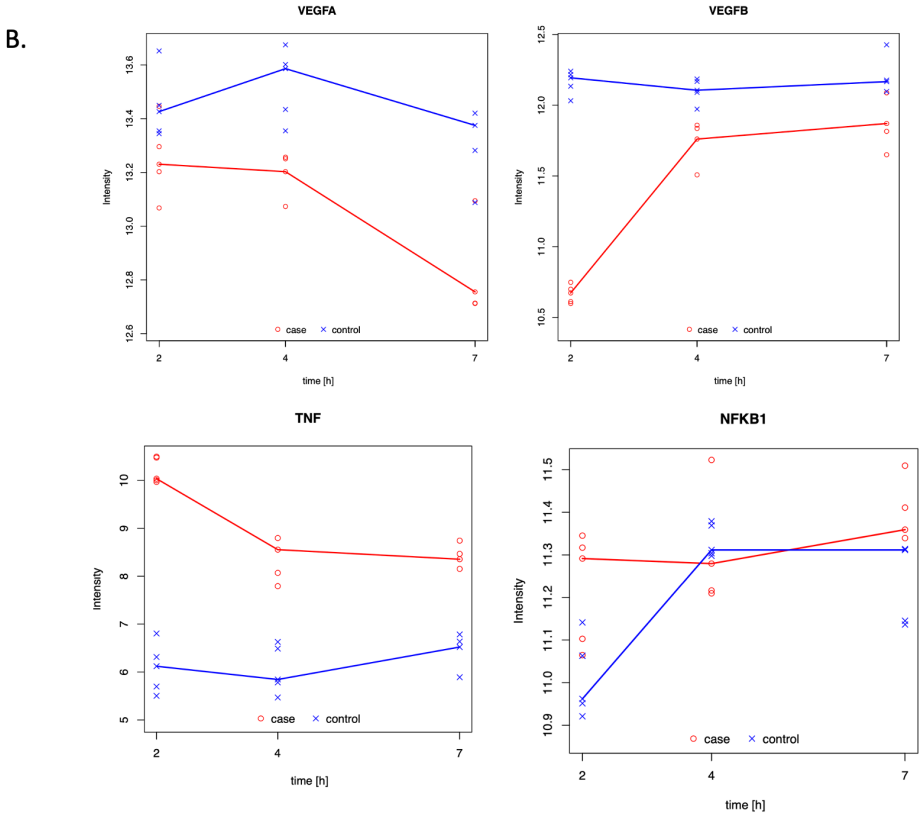

C.

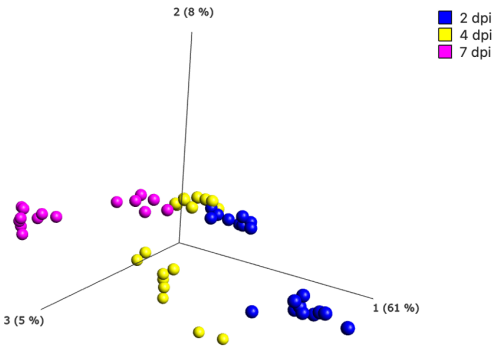

922/29649 Variables

Filter by Fold Change	1
t-test [≠] time 2 dpi, 7 dpi	p = 1.00e-06 q = 3.20e-05
Eliminated factors	None
Filter by Standard Deviation (s/s_{max})	0
Variable list input	No
Active Samples	52/52
Normalization	Mean=0,Var=1
Missing value reconstruction	N/A
Collapse mode	none

D.

Index	Name BioCarta 2016	P-value	Adjusted p-value	Odds Ratio	Combined score
1	CBL mediated ligand-induced downregulation of EGF receptors Homo sapiens h cblPathway	0.002272	0.1026	16.13	98.18
2	Eukaryotic protein translation Homo sapiens h eifPathway	0.001249	0.1026	10.77	71.97
3	IL 6 signaling pathway Homo sapiens h il6Pathway	0.01014	0.1724	8.06	37.02
4	Sprouty regulation of tyrosine kinase signals Homo sapiens h spryPathway	0.005092	0.1113	6.73	35.51
5	Role of ERBB2 in Signal Transduction and Oncology Homo sapiens h her2Pathway	0.002944	0.1026	5.85	34.12
6	Beta-arrestins in GPCR Desensitization Homo sapiens h bArrestinPathway	0.002944	0.1026	5.85	34.12
7	VEGF, Hypoxia, and Angiogenesis Homo sapiens h vegfPathway	0.004023	0.1026	5.39	29.71
8	mCalpain and friends in Cell motility Homo sapiens h mCalpainPathway	0.004023	0.1026	5.39	29.71

E.

Index	Name COVID-19 Related Gene Sets 2021	P-value	Adjusted p-value	Odds Ratio	Combined score
1	COVID19-Nsp13 protein host PPI from Krogan	0.0004283	0.006624	5.91	45.80
2	SARS coronavirus nsp3-pp1a/pp1ab (gene: orf1ab) from Virus-Host PPI P-HIPSTer 2020	0.00001801	0.001393	4.04	44.14
3	419 proteins down-regualated at 2h in SARS-CoV-2 infected cells from Bouhaddou et al. 2020	4.157e-7	0.0001929	2.71	39.80
4	SARS coronavirus nsp9-pp1a/pp1ab (gene: orf1ab) from Virus-Host PPI P-HIPSTer 2020	0.01014	0.05957	8.06	37.02
5	277 proteins down-regualated at 0h in SARS-CoV-2 infected cells from Bouhaddou et al. 2020	0.000005892	0.0009113	2.91	35.05
6	SARS coronavirus P2 envelope protein from Virus-Host PPI P-HIPSTer 2020	0.01257	0.06935	7.33	32.08
7	SARS coronavirus protein E (gene: E) from Virus-Host PPI P-HIPSTer 2020	0.01257	0.06935	7.33	32.08
8	Top 500 down genes for SARS-CoV-2 late-stage infection in human male blood from GSE161731	0.000001855	0.0004304	2.43	32.05
9	SARS coronavirus excised polyprotein 1..4369 (gene: orf1ab) from Virus-Host PPI P-HIPSTer 2020	0.00005500	0.001823	3.05	29.88
10	184 proteins up-regualated at 0h in SARS-CoV-2 infected cells from Bouhaddou et al. 2020	0.0001057	0.003066	2.99	27.36

Figure 2. Analysis from a pulmonary murine (WT) study involving analysing lung tissue (GSE68820) is shown. MA15 versus Mock nasal instillation was compared. Comparing day 2 and 7 VEGF-A, TNF and NFKB1 gene-expression is significantly down regulated and VEGFB is significantly up-regulated (Figure 1A). TTCA plots suggest trends in VEGFA and VEGFB gene expression (Figure 1B). TTCA demonstrate increased intensity compared to controls for TNF gene expression (day two to day

seven), whereas for NFKB1 gene expression controls and cases converge by day four. Two days versus 7 days post instillation (DPI) yields a t-test on the 52 samples, filtering to 922 genes (p=1.00e-06 and q= 3.20e-05) , with qluclore in the non collapsed mode (Figure 1C). When this gene list is parsed through pathway analysis using the Enrichr online platform (https://maayanlab.cloud/Enrichr/enrich#) 720 genes are noted to be unique. Thereby pathway enrichment analysis elicits BioCarta2016 and pathways consisting of IL-6 signalling and 'VEGF, Hypoxia and Angiogenesis' (Figure 1D). Also, Enrichr enriches pathways containing Covid-19 related genes (Figure 1E).

Figure 3: Murine Pulmonary effects of Varying MA15 doses as assessed by VEGF-A, VEGF-B, TNF and NFKB1 gene expression.

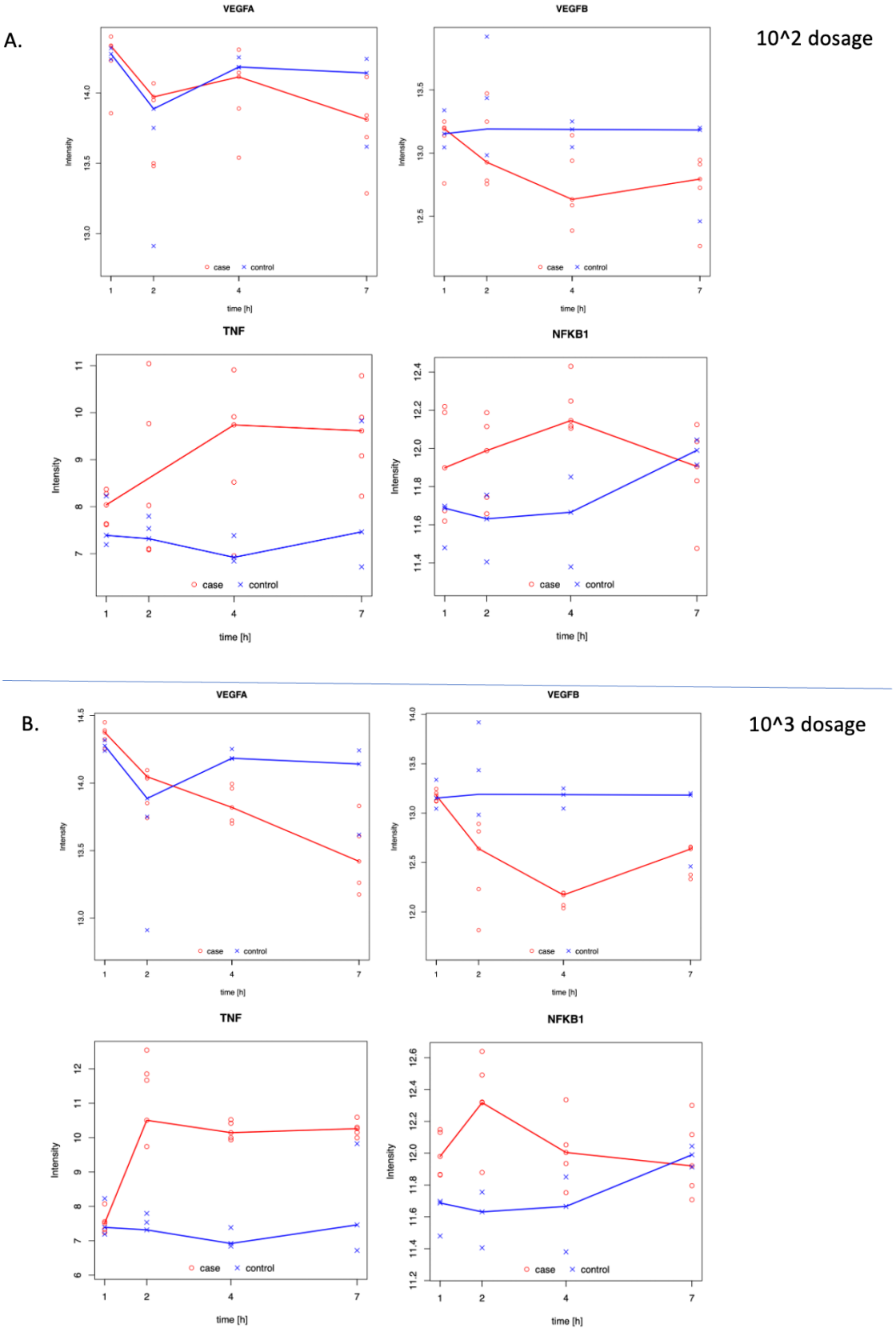

C.

10^4 dosage

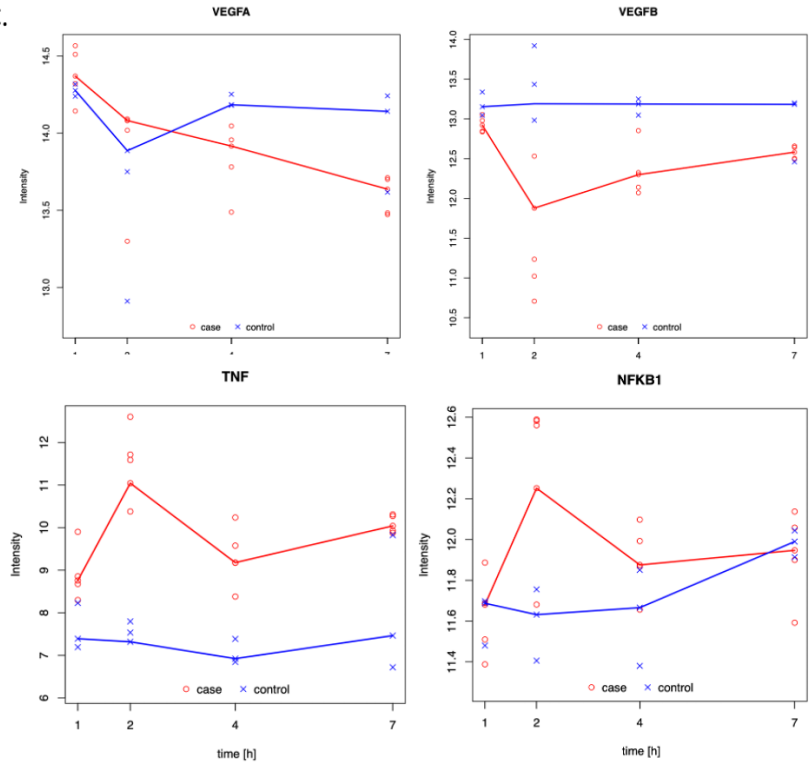

D.

10^5 dosage

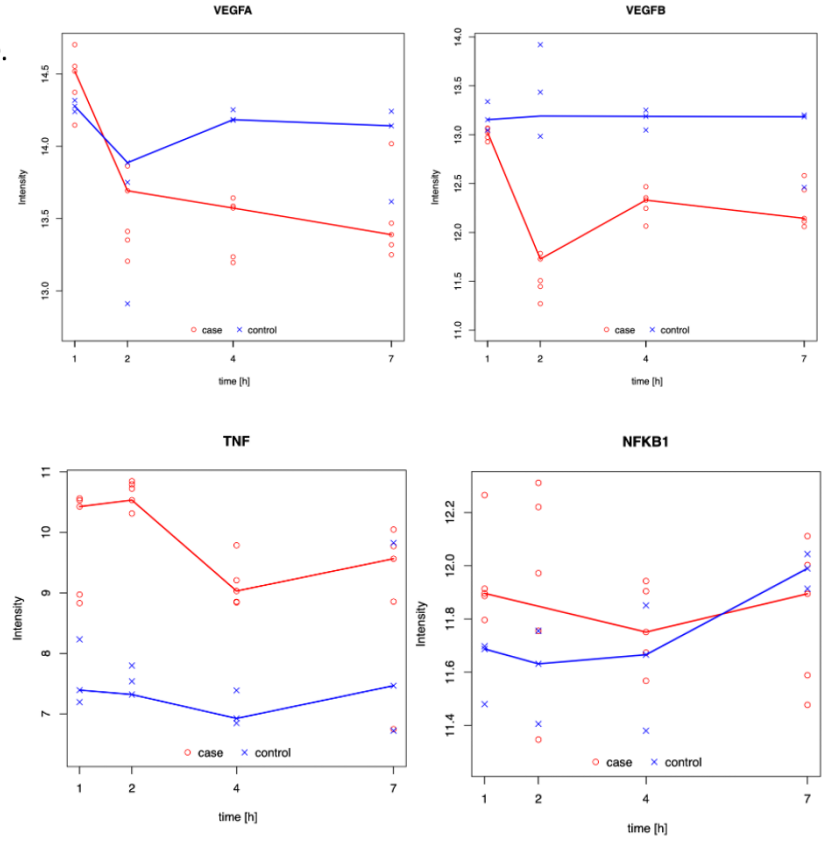

E.

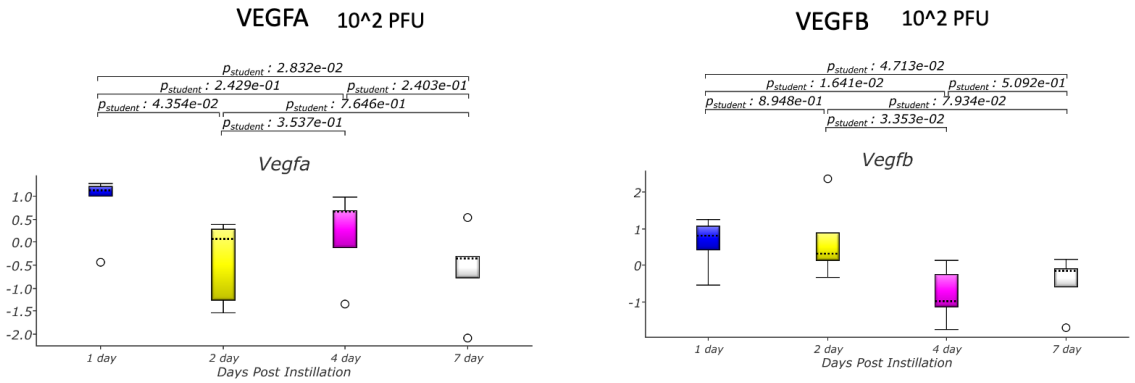

F.

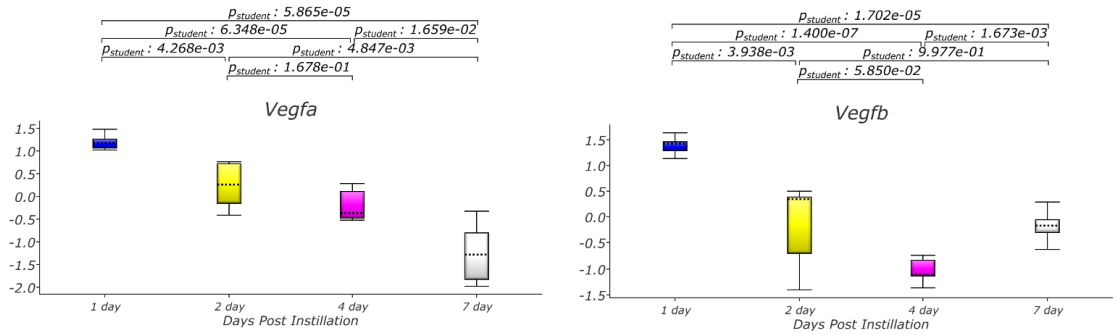

G.

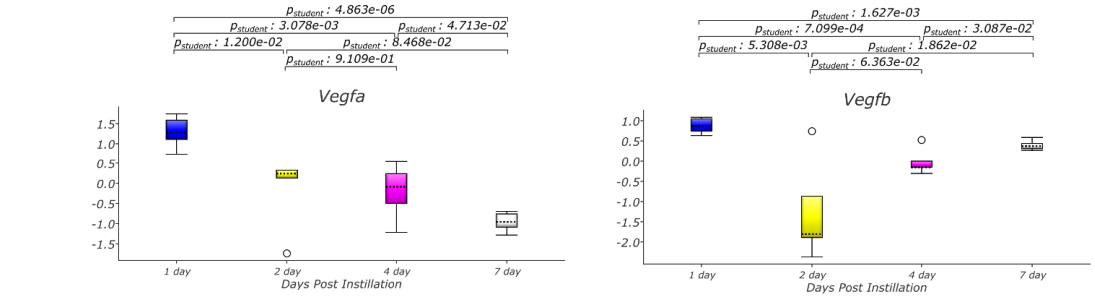

H.

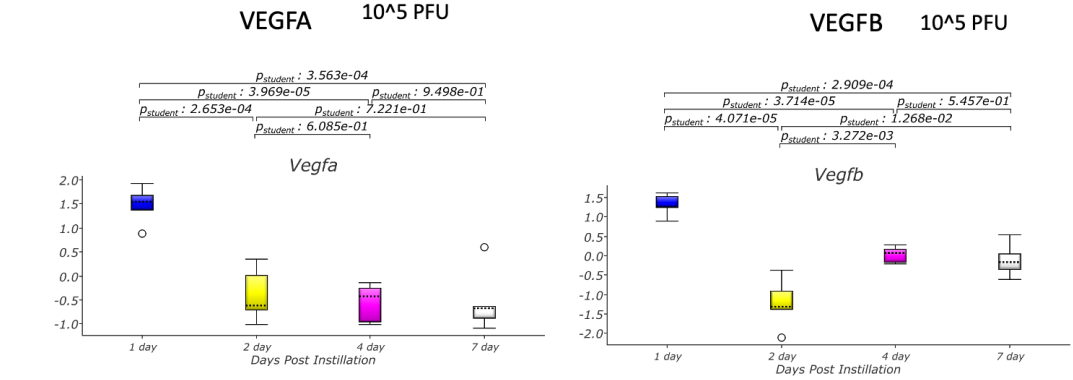

Figure 3 A-D. A temporal study (**GSE33266)** after SARS COV MA15 nasal instillation at varying MA15 doses (10^2, 10^3, 10^4 and 10^5) is shown. NFKB1, TNF, VEGFA and VEGFB gene expression (GE) is illustrated by TTCA (A-D) and box plot (E-H) analysis. TTCA **VEGF-A** GE diverges in intensity between controls (Mock) and cases (MA15 stimulated) in intensity (Day 4 to 7). **TTCA/VEGF-B** GE: a fall is noted by two hours at all MA15 dosing, followed by further fall for the 10^2 and 10^3 doses and then an increase in intensity is noted across all profiles. **TTCA/TNF** GE, a significant divergence is noted across all categories, comparing controls and cases, which remains throughout the profiles. Whereas, for **TTCA/NFKB1** GE, controls and cases converge with increasing time. Trends in NFKB1 and TNF gene expression showed 10^3 and 10^4 PFU dosing resulting in an increase in NFKB1 gene expression between day 1 and day 2, suggesting an acute inflammatory response. Box plot **VEGF-A** gene expression: 10^2 dose (no change GE), at 10^3, 10 ^4 and 10^5 a significant decrease in GE is noted (Day 1 compared to Day 7). Box plot **VEGF-B** gene expression: at 10^2 (no change GE), for 10^3 a significant fall is noted at 10^3, 10 ^4 and 10^5 doses (Day 1 to Day 7), however both the 10^4 and 10^5 dose show a ‘v’ shape at Day 1, Day 2 and Day 4 vertices.

Figure 4: Affect of Differing Antigenic Patterns of Pulmonary Gene Expression in the WT Murine Model.

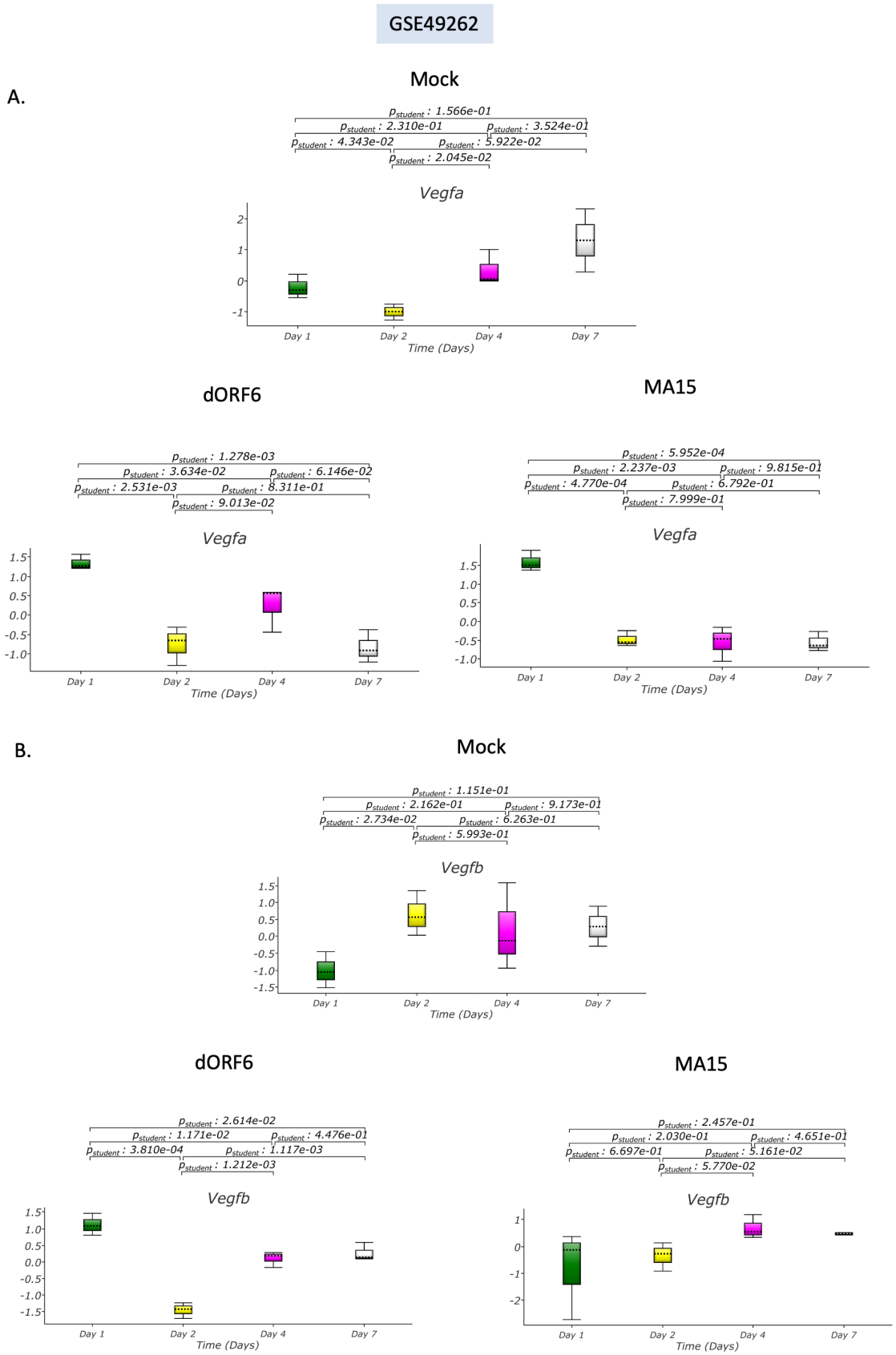

GSE49263

C.

Mock

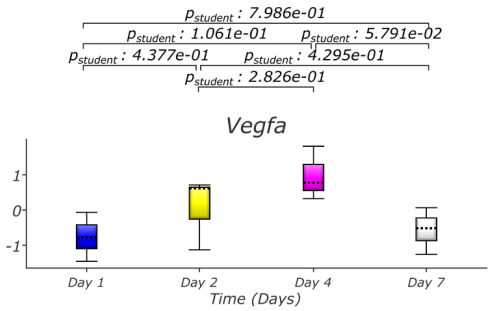

nsp16

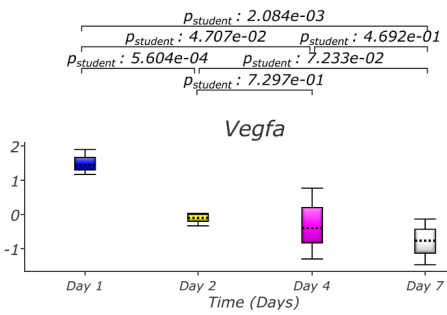

MA15

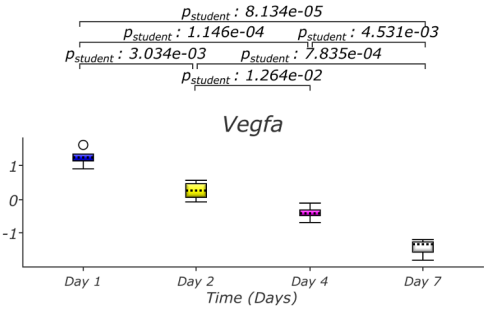

D.

Mock

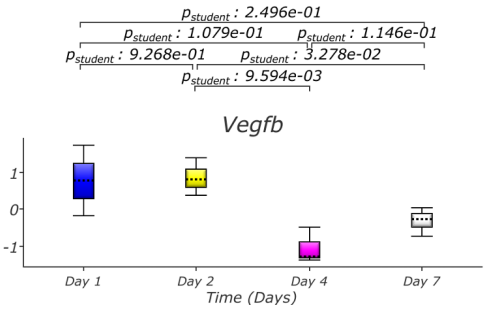

nsp16

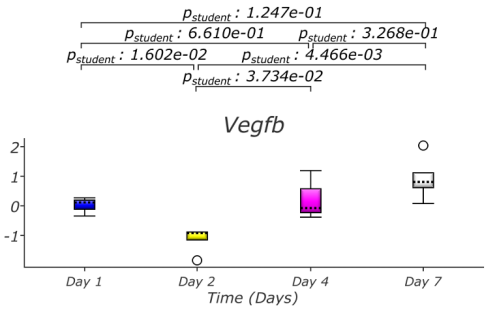

MA15

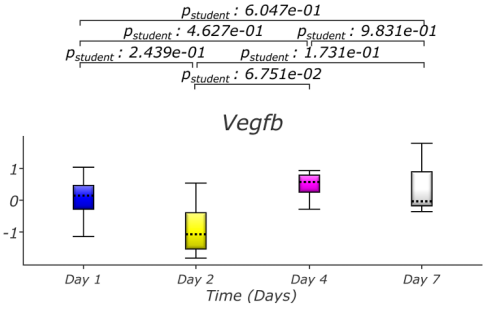

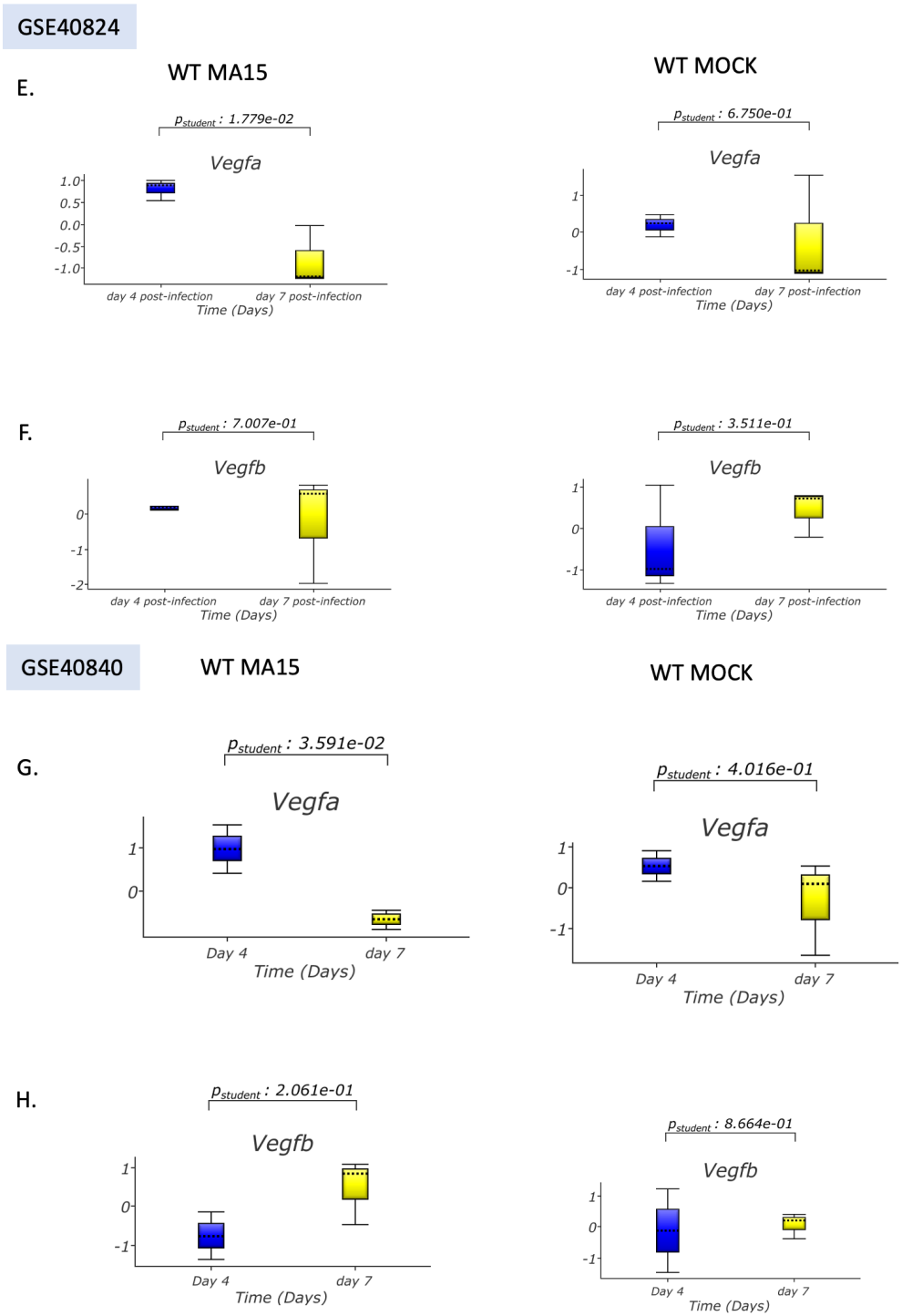

Figure 4. Stimulation of WT Mice with either Mock, dORF6 or MA15 as shown (edit illustration). VEGF-A Gene Expression (GE) (Figure 4A,C,E and G) and VEGF-B GE (Figure 4B,D, F and H) is illustrated. **Dataset GSE49262** shows Day 1 to Day 7 with a significant fall in VEGF-A GE for dORF6 and MA15, with no change for Mock. Also for VEGF-B only dORF6 shows a significant fall between Day 1 and day 7, and a significant rise in GE between Day 2 and 4. **Dataset GSE49263** shows a significant fall in VEGF-A (Day1 to Day5) after nsp16 and MA15 stimulation. For VEGF-B GE is not differentiated between the start and the finish of all studies. Dataset **GSE40824** and **GSE40840** VEGF-A GE shows a fall, with no change for VEGF-B GE.

Figure 5: VEGFA, VEGFB Gene Expression, 10^4 Versus 10^5 MA15 instillation in the Pulmonary Murine WT model

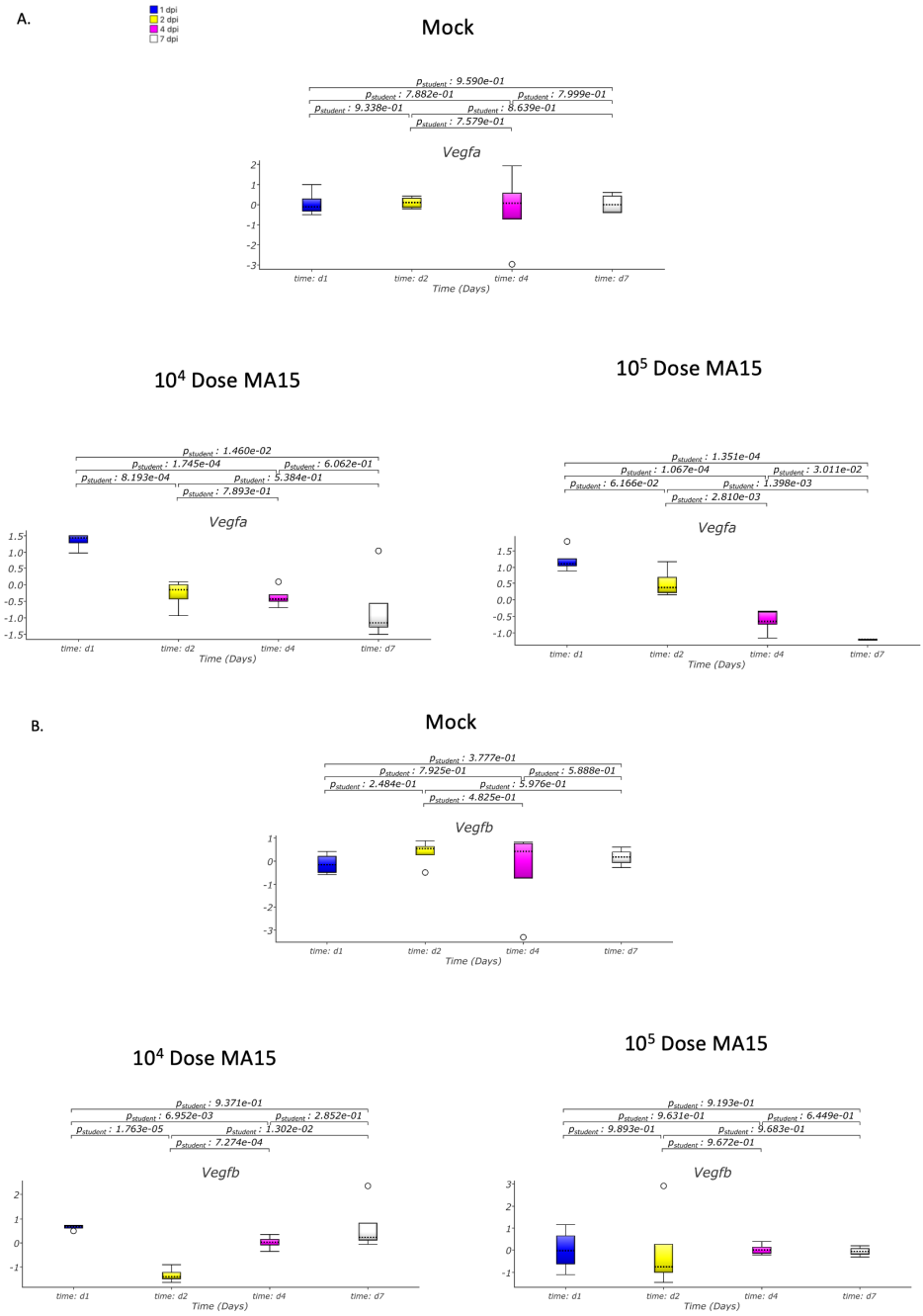

Figure 5. Murine MA15 nasal instillation studies are illustrated. Box plots are show for study datasets GSE50000 (Figure 4A), with gene expression (GE) temporal profiles shown for VEGF-A and VEGFB. Both the 10^4 and 10^5 MA15 doses lead to a fall in VEGF-A GE, with the fall being more significant at the10^5 dose (Figure 5A). There was no change from mock to the increasing MA15 doses for VEGF-B GE (Day 1 compared to Day 7) (Figure 5B).

Figure 6. VEGF Receptors Docking for Spike Protein of SARS-CoV

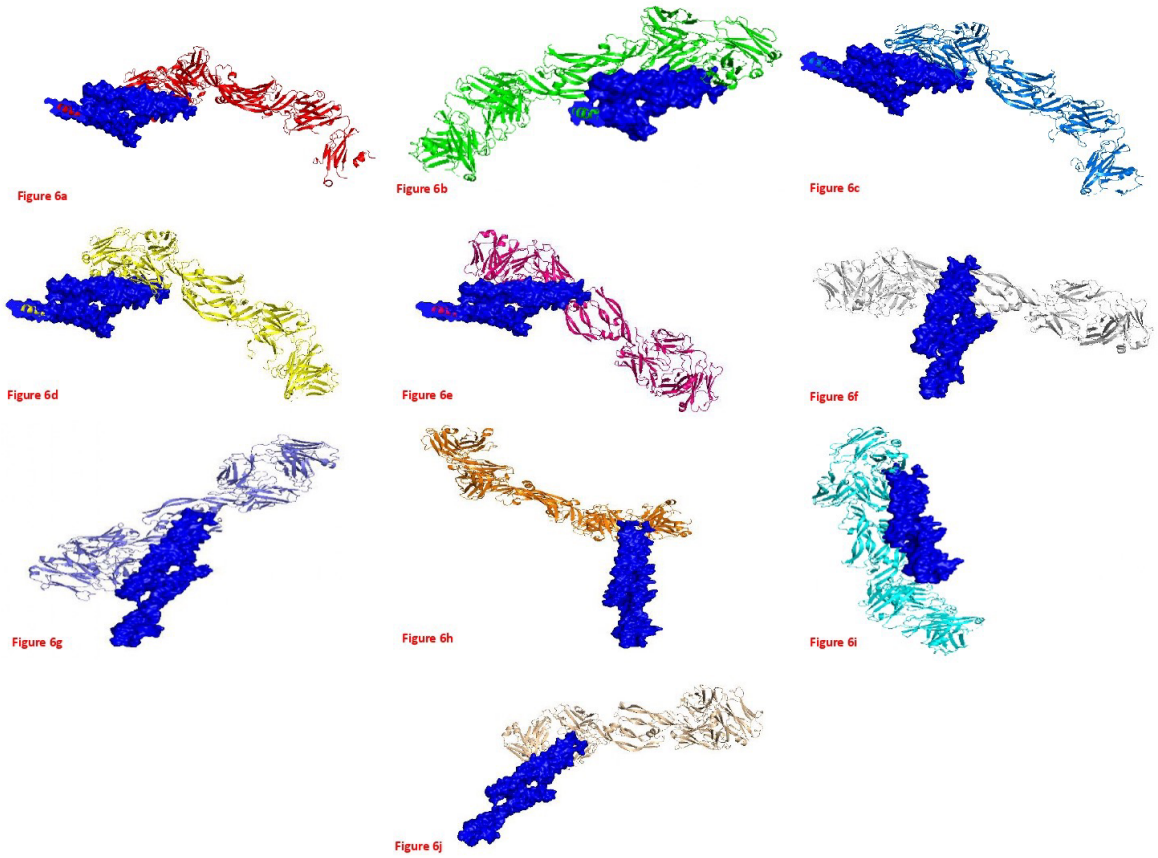

Figure 6: Docking of VEGFA and VEGFB receptors were modelled and docked with ligands of Spike protein of SARS-CoV, the best ten models were finalised on the basis of best scored by electrostatics and desolvation energy. *In silico* protein protein interaction signifies that VEGF protein shows stable interaction which may have pathological consequences.

Figure 7: Mechanistic Model of Temporal VEGF-A and VEGF- B changes in Gene Expression, with Pathophysiological Consequences

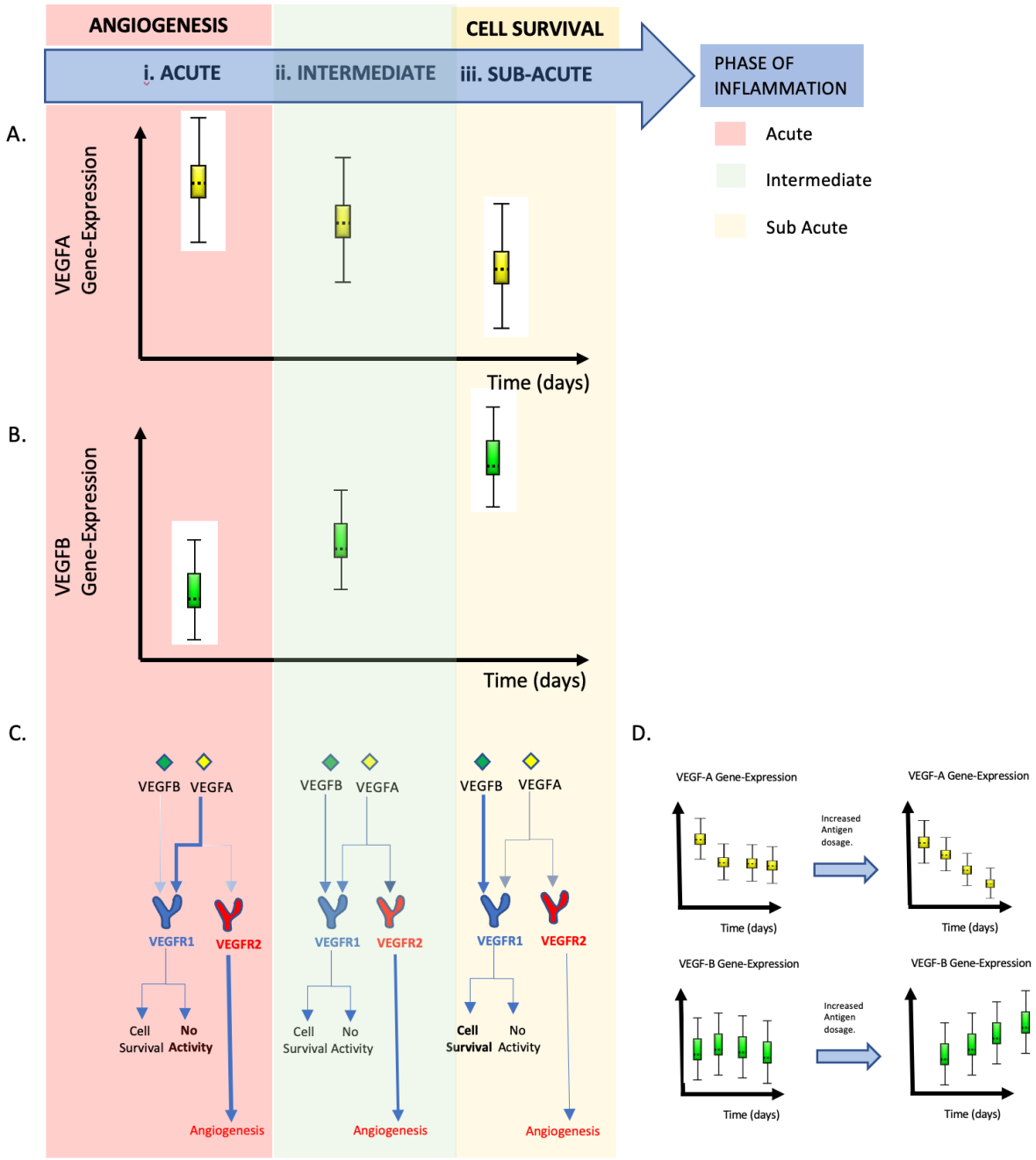

Figure 7. This schematic represents VEGF-A and VEGF-B interactions post-SARS-CoV infection in the pulmonary Murine model. Temporal differences in VEGF-A and VEGF-B gene expression are illustrated **(Figures 4A and B)**. In the diagram **(Figure 4C),** three states are depicted, 'Acute,' 'Intermediate,' and 'Sub Acute,' which are suggested to switch over days. In the acute state, the rise in VEGF-A results in angiogenesis from VEGFR-2 stimulation. Then in the intermediate state, cell survival and angiogenesis may be in equipoise. Finally, in the Subacute state, the lower level of VEGF-A diminished angiogenesis with enhanced VEGF-B levels enhancing cell survival due to biding with VEGFR-1. The research undertaken in this paper has shown that the magnitude of antigen dosing affected the temporal gene-expression trajectory; we suggest driving to patterns of VEGF-A and VEGF-B GE as depicted in the diagram shown (**Figure 4D**).

TABLE 1: Study characteristics of WT Pulmonary Study after MA15 nasal instillation

GSE	Number of MA15 instilled animals	Number of Mock Instilled	The dose of SARS-CoV MA15 (PFU) Instilled	Age of Mice (weeks)	Time points (DPI)
51387	5	4	10^5	20	4,7
51386	7	8	10^4	20	4,7
50878	8	9	10^5	10	2,4,7
50000	32	16	10^4 or 10^5	20	1,2,4,7
49263	15	11	10^5	20	1,2,4,7
49262	12	11	10^5	20	1,2,4,7
40840	10	10	10^5	10	4,7
40827	9	10	10^5	10	4.7
40824	11	11	10^5	10	4,7
36016	9	3	10^5	10	2,5,9
68820	28	24	10^4	10	2,4,7
33266	25	12	10^2,10^3, 10^4, 10^5	20	1,2,4,7

Table 1. Ten and Twenty-week-old mice were infected by intranasal instillation of 10^5 or 10^4 PFU of SARS MA15 in 50 ¬µl of PBS or mock-infected with PBS alone. Lungs were then harvested at the above time points according to Days Post Infection (DPI). The GSE number is the NCBI database identifier for the concerned study. GSE33266 and GSE68820 were studies performed by the same research group. GSE33266 concentrates on dose effects and the GSE68820 on temporal changes and their analysis data is shown (Figure 2 and Figure 3, respectively).

TABLE 2: Protein-Protein docking models ranked assigned after docking between VEGF and S Protein of SARS-CoV

PDB_ID assigned	Electrostatics	Desolvation	VdW	Rank
63	-13.043	7.302	50.613	1
3435	-2.424	8.406	0.355	2
8680	-1.75	2.569	18.595	3
3391	-27.19	-12.583	40.827	4
2220	-1.938	-10.929	37.028	5
137	-18.51	12.592	73.641	6
46	-16.967	13.261	52.751	7
9467	-9.389	-0.944	38.844	8
7466	-3.91	-7.487	53.152	9
3266	-17.419	-19.212	63.071	10

Table 2. A study of VEGF and SARS-CoV protein binding, using Vander wall forces (VdW).

References

1. Martínez-Colón GJ, Ratnasiri K, Chen H, et al. SARS-CoV-2 infection drives an inflammatory response in human adipose tissue through infection of adipocytes and macrophages. *Science Translational Medicine.*0(0):eabm9151.
2. Ravichandran B, Grimm D, Krüger M, Kopp S, Infanger M, Wehland M. SARS-CoV-2 and hypertension. *Physiological Reports.* 2021;9(11):e14800.
3. Harrison AG, Lin T, Wang P. Mechanisms of SARS-CoV-2 Transmission and Pathogenesis. *Trends in Immunology.* 2020;41(12):1100-1115.
4. Yin XX, Zheng XR, Peng W, Wu ML, Mao XY. Vascular Endothelial Growth Factor (VEGF) as a Vital Target for Brain Inflammation during the COVID-19 Outbreak. *ACS Chem Neurosci.* 2020;11(12):1704-1705.
5. Chi Y, Ge Y, Wu B, et al. Serum Cytokine and Chemokine Profile in Relation to the Severity of Coronavirus Disease 2019 in China. *J Infect Dis.* 2020;222(5):746-754.
6. Otrock ZK, Makarem JA, Shamseddine AI. Vascular endothelial growth factor family of ligands and receptors: Review. *Blood Cells, Molecules, and Diseases.* 2007;38(3):258-268.
7. Razavi ZS, Asgarpour K, Mahjoubin-Tehran M, et al. Angiogenesis-related non-coding RNAs and gastrointestinal cancer. *Molecular Therapy - Oncolytics.* 2021;21:220-241.
8. Lal N, Puri K, Rodrigues B. Vascular Endothelial Growth Factor B and Its Signaling. *Frontiers in Cardiovascular Medicine.* 2018;5.
9. Peach CJ, Mignone VW, Arruda MA, et al. Molecular Pharmacology of VEGF-A Isoforms: Binding and Signalling at VEGFR2. *International Journal of Molecular Sciences.* 2018;19(4):1264.
10. Rovas A, Osiaevi I, Buscher K, et al. Microvascular dysfunction in COVID-19: the MYSTIC study. *Angiogenesis.* 2021;24(1):145-157.
11. Stookey JD, Allu PKR, Chabas D, Pearce D, Lang F. Hypotheses about sub-optimal hydration in the weeks before coronavirus disease (COVID-19) as a risk factor for dying from COVID-19. *Medical hypotheses.* 2020;144:110237-110237.
12. Zafar Mohammad I, Zheng J, Kong W, et al. The role of vascular endothelial growth factor-B in metabolic homoeostasis: current evidence. *Bioscience Reports.* 2017;37(4).
13. Abe I, Islam F, Lo CY, Liew V, Pillai S, Lam AK. VEGF-A/VEGF-B/VEGF-C expressions in non-hereditary, non-metastatic phaeochromocytoma. *Histol Histopathol.* 2021;18:18329.
14. Ackermann M, Mentzer SJ, Kolb M, Jonigk D. Inflammation and intussusceptive angiogenesis in COVID-19: everything in and out of flow. *Eur Respir J.* 2020;56(5).
15. Madureira G, Soares R. The misunderstood link between SARS-CoV-2 and angiogenesis. A narrative review. *Pulmonology.* 2021.
16. Dabravolski SA, Khotina VA, Omelchenko AV, Kalmykov VA, Orekhov AN. The Role of the VEGF Family in Atherosclerosis Development and Its Potential as Treatment Targets. *International Journal of Molecular Sciences.* 2022;23(2):931.
17. Olofsson B, Pajusola K, Kaipainen A, et al. Vascular endothelial growth factor

B, a novel growth factor for endothelial cells. *Proceedings of the National Academy of Sciences.* 1996;93(6):2576-2581.
18. Rashid A, Toufiq M, Khilnani P, et al. VEGF subtype A and B Gene Expression, Clues to a Temporal Signature in Kawasaki Disease, Implications for Coronary Pathogenesis through a Secondary analysis of Clinical Datasets. *medRxiv.* 2022:2022.2008.2008.22278559.
19. Roberts A, Deming D, Paddock CD, et al. A mouse-adapted SARS-coronavirus causes disease and mortality in BALB/c mice. *PLoS Pathog.* 2007;3(1):e5.
20. SchrödingerLLC. he PyMOL Molecular Graphics System, Version 1.2r3pre, Schrödinger, LLC.
21. Albrecht M, Stichel D, Muller B, et al. TTCA: an R package for the identification of differentially expressed genes in time course microarray data. *BMC Bioinformatics.* 2017;18(1):33.
22. Li X, Lee C, Tang Z, et al. VEGF-B: a survival, or an angiogenic factor? *Cell Adh Migr.* 2009;3(4):322-327.
23. Lal N, Puri K, Rodrigues B. Vascular Endothelial Growth Factor B and Its Signaling. *Front Cardiovasc Med.* 2018;5:39.
24. Moutal A, Martin LF, Boinon L, et al. SARS-CoV-2 spike protein co-opts VEGF-A/neuropilin-1 receptor signaling to induce analgesia. *Pain.* 2021;162(1):243-252.
25. Farzaneh Behelgardi M, Zahri S, Mashayekhi F, Mansouri K, Asghari SM. A peptide mimicking the binding sites of VEGF-A and VEGF-B inhibits VEGFR-1/-2 driven angiogenesis, tumor growth and metastasis. *Scientific Reports.* 2018;8(1):17924.
26. Sadremomtaz A, Ali AM, Jouyandeh F, et al. Molecular docking, synthesis and biological evaluation of Vascular Endothelial Growth Factor (VEGF) B based peptide as antiangiogenic agent targeting the second domain of the Vascular Endothelial Growth Factor Receptor 1 (VEGFR1D2) for anticancer application. *Signal Transduction and Targeted Therapy.* 2020;5(1):76.
27. Ghasemali S, Farajnia S, Barzegar A, et al. Rational Design of Anti-Angiogenic Peptides to Inhibit VEGF/VEGFR2 Interactions for Cancer Therapeutics. *Anti-Cancer Agents in Medicinal Chemistry (Formerly Current Medicinal Chemistry-Anti-Cancer Agents).* 2022;22(10):2026-2035.
28. Korpela H, Lampela J, Airaksinen J, et al. AAV2-VEGF-B gene therapy failed to induce angiogenesis in ischemic porcine myocardium due to inflammatory responses. *Gene Therapy.* 2022:1-10.